


Colloidal Synthesis of $\text{Cu}_2\text{CdSnSe}_4$ Nanocrystals and Hot-Pressing to Enhance the Thermoelectric Figure-of-Merit

Feng-Jia Fan,^{†,‡} Bo Yu,^{‡,‡} Yi-Xiu Wang,[†] Yan-Long Zhu,[†] Xiao-Jing Liu,[†] Shu-Hong Yu,^{*,†} and Zhifeng Ren^{*,‡}

[†]Division of Nanomaterials & Chemistry, Hefei National Laboratory for Physical Sciences at Microscale, Department of Chemistry, National Synchrotron Radiation Laboratory, University of Science and Technology of China, Hefei 230026, P.R. China

[‡]Department of Physics, Boston College, Chestnut Hill, Massachusetts 02467, United States

 Supporting Information

ABSTRACT: We report a solution-based synthesis of monodispersed $\text{Cu}_2\text{CdSnSe}_4$ nanocrystals and a study on the thermoelectric properties of these wide-band-gap dense materials compacted from nanocrystals for the first time. With the help of copper dopants and selenium vacancies generated during wet-chemistry synthesis, a large increment in the power factor is observed, and the dimensionless figure-of-merit ZT reaches a peak value of 0.65 at 450 °C.

During the past few decades, ongoing efforts have been devoted to improving the performance of thermoelectric (TE) materials for their important applications in cooling and power generation.¹ Ideal TE materials possess low thermal conductivity, like glass, with good electrical conductivity, like crystals. Compacting wet-chemistry-synthesized nanoparticles into dense samples is expected to be an efficient strategy to achieve low thermal conductivity due to the enhanced scattering of phonons at the numerous grain boundaries, and at the same time samples with high density after compaction could also show increased thermopower.² Recently, many studies on dense materials compacted from wet-chemistry-synthesized nanostructures, such as Bi_2Te_3 ,³ Bi_2Te_3 ,⁴ and $\text{Bi}_{2-x}\text{Sb}_x\text{Te}_3$,⁵ have reported that they show depressed thermal conductivities compared with bulk materials, and for those semimetal or narrow-band-gap semiconductors, deteriorations in electric conductivity and further adverse effects on the power factor are also obvious. There are few reports representing any enhancement in the final dimensionless figure-of-merit value (ZT).^{5d,6}

Recently, novel quaternary chalcogenide $\text{Cu}_2\text{CdSnSe}_4$ (CCTSe)⁷ and other chalcogenides with wide band gaps, such as $\text{Cu}_2\text{ZnSnSe}_4$ ⁸ and Cu_2SnSe_3 ,⁹ have been found to have reasonable thermoelectric properties at medium temperatures when doped with Cu or In. For Cu-doped CCTSe, even though it has a relatively low electrical conductivity compared with those of traditional small-band-gap TE materials, a reasonable ZT value could still be achieved because the diverse types of bonding inside the compound lead to a naturally distorted structure that can scatter more phonons, resulting in a low thermal conductivity. Furthermore, wet-chemistry synthesis of these quaternary chalcogenide nanocrystals and their subsequent compaction into dense samples could also benefit from increased grain boundaries to further reduce the thermal conductivity, as lattice thermal conductivity dominates the total thermal conductivity of CCTSe

and, on the other hand, proper dopants (which can be tuned in wet-chemistry synthesis) can be effective in enhancing the power factor,⁷ which makes this route a promising and straightforward approach to the ideal model of “phonon-glass and electron-crystal”. To the best of our knowledge, the colloidal syntheses of monodispersed ternary and quaternary chalcogenide nanocrystals such as CuInS_2 ,¹⁰ CuInSe_2 ,¹¹ and $\text{Cu}_2\text{ZnSnS}_4$ ¹² have been a hot issue due to their potential as inorganic solar absorbers in photovoltaics and photodetector devices. However, colloid-based syntheses of monodispersed CCTSe nanoparticles and the study of the thermoelectric properties of dense materials compacted from CCTSe nanoparticles are still unknown.

In this Communication, we report the first solution-based strategy for controlled synthesis of monodispersed CCTSe nanocrystals, and we prepare dense CCTSe materials by compressing those wet-chemistry-synthesized nanocrystals. For this wide-band-gap semiconductor, copper dopants and selenium vacancies generated during the chemical synthesis process are effective in enhancing the power factor; thus, a high peak ZT value of 0.65 can be obtained at 450 °C.

The nanocrystals were prepared through an oleylamine- and 1-octadecene-mediated solvothermal synthesis, with typical yields of about 1 g per run. The capping ligands on the nanocrystals were removed via a procedure modified from a previously reported route,^{4a} and then more than 11 g of as-prepared surface-clean nanoparticles were hot-pressed (uniaxial pressure of 80 MPa at 550 °C for 0.5 h) into a bulk cylindrical sample with a diameter of 12.5 mm and a height of more than 13 mm. The density of the obtained sample (5.7 g cm^{-3}) is up to 95% of the theoretical value.

The composition of the synthesized CCTSe nanoparticles was determined by inductively coupled plasma (ICP) analysis can be described as $\text{Cu}_{2.1}\text{Cd}_{0.8}\text{SnSe}_{3.4}$, from which we can see that those nanocrystals are copper rich and selenium as well as cadmium insufficient.

The PXRD pattern in Figure 1a can be indexed as stannite-type CCTSe (JCPDS52-0869), and the unit cell is presented in the inset of Figure 1b, which shows an element distribution similar to that of cubic ZnSe. The Cu_xSe and Cu_2SnSe_3 phases show diffraction patterns similar to those of CCTSe, and they are difficult to distinguish from the majority phase here due to peak broadening. Room-temperature Raman spectra are obtained as well to confirm the phase of the as-prepared nanocrystals. In the

Received: July 30, 2011

Published: September 12, 2011

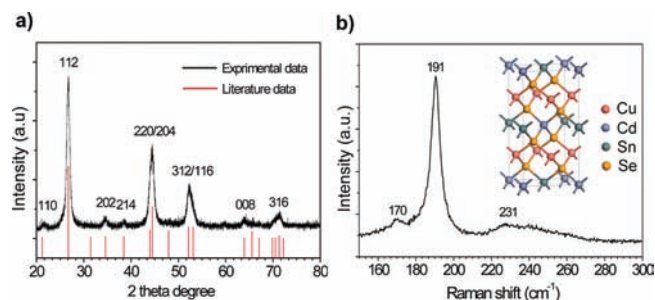


Figure 1. (a) XRD patterns and (b) Raman spectra of the prepared CCTSe nanocrystals. The inset in (b) shows a unit cell of the stannite-type CCTSe crystal.

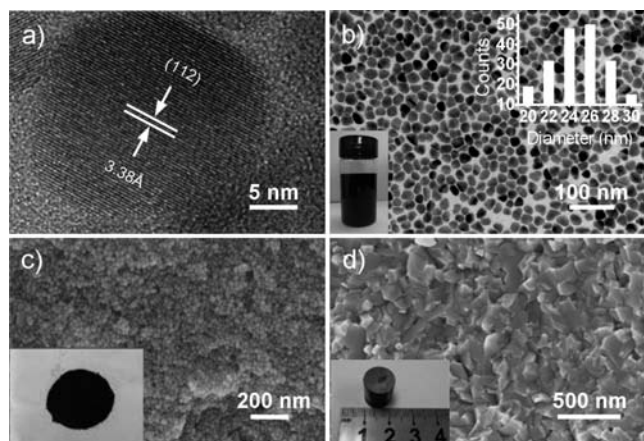


Figure 2. (a) HRTEM image of a single CCTSe nanocrystal, showing that it is well crystallized. (b) A general overview TEM image of CCTSe nanocrystals. The insets in (b) show size distributions observed from TEM images and a photograph of nanocrystals dispersed in hexane. (c) SEM image showing the surface-clean CCTSe nanoparticles. (d) SEM image of CCTSe dense material after hot pressing. The insets in (c) and (d) show photographs of the surface-clean CCTSe nanocrystals powder and the hot-pressed CCTSe cylinder.

region of $150\text{--}300\text{ cm}^{-1}$, Cu_2SnSe_3 and Cu_xSe exhibit the most intense peaks at 180 and $260\text{--}265\text{ cm}^{-1}$, respectively, while the CCTSe phase shows peaks similar to those of $\text{Cu}_2\text{ZnSnSe}_4$ at $170\text{--}171$ and $194\text{--}196\text{ cm}^{-1}$, together with a less intense peak at 231 cm^{-1} that is sensitive to variations in the composition.¹³ Three peaks located at 170 , 191 , and 231 cm^{-1} here match well with those for a tetragonal CCTSe phase, with some red-shift due to defects and the size effect.¹⁴ Raman peaks with respect to Cu_2SnSe_3 or Cu_xSe are hard to find. Peak-broadening at 231 cm^{-1} indicates that there are composition variations among different nanocrystals. As CdSe could be excluded on the basis of the XRD patterns, we confirm that the obtained nanocrystals are tetragonal CCTSe rather than a mixture of binary or ternary chalcogenides.

The size distribution and morphologies of the CCTSe nanocrystals are presented in Figure 2b; their diameters are in the range of $20\text{--}30\text{ nm}$. The HRTEM image in Figure 2a obtained on a typical CCTSe single nanocrystal indicates that it is well crystallized, and the lattice space of 3.38 \AA in Figure 1a corresponds to that for the (112) face of tetragonal CCTSe. SEM images of the surface-clean nanoparticles and the hot-pressed cylinder are presented in Figure 2c,d. The surface-clean

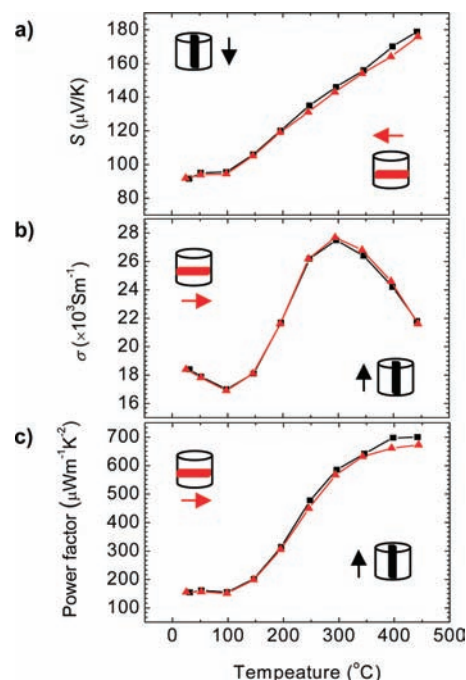


Figure 3. Temperature dependence of (a) electric conductivity, (b) Seebeck coefficient, and (c) power factor parallel and perpendicular to the hot-pressing direction. Arrows indicate the directions of the property being measured; the direction of the hot pressing is parallel to the black arrows.

nanocrystals have uniform diameters over a large scale; regrowth of CCTSe nanoparticles could be observed after the hot-pressing process. According to calculations (Supporting Information, Figure S3) based on the Debye–Scherrer equation, the crystalline domains after hot-pressing should be about 40 nm . The ultrathin TEM image and corresponding selected area electron diffraction (SAED) rings in Figure S1 also indicate that the large grains with diameters of several hundred nanometers observed by SEM are actually composed of smaller features.

Room-temperature UV–vis spectra show that CCTSe nanocrystals dispersed in hexane have strong absorbance in the visible light region (Figure S2). The energy band gap of as-prepared CCTSe nanocrystals, extrapolated from the UV–vis spectra, is about 1.1 eV , which is a little larger than previously reported due to the size effect.^{7,13b}

Two bar samples (parallel and perpendicular to the hot-press directions) were cut separately from the hot-pressed cylinder, and their electrical conductivity (σ) and Seebeck coefficients (S) were measured accordingly. As shown in Figure 3a, σ of the CCTSe dense sample shows similar temperature dependence in both directions. In the perpendicular direction, the highest conductivity of $27\,700\text{ S m}^{-1}$, observed at $300\text{ }^\circ\text{C}$, is much larger than that of undoped CCTSe bulk polycrystalline material and about 10% larger than the state-of-the-art value observed in polycrystalline $\text{Cu}_{2.1}\text{Cd}_{0.9}\text{SnSe}_4$ bulk material.⁷ Previous research found that Cu-doped CCTSe bulk materials showed drastic enhancement of σ , and the improvements were attributed to the creation of p-type carriers.⁷ Herein, besides the copper dopants, the selenium vacancies in our dense material would further increase the carrier concentration. The peak Seebeck coefficients in the directions perpendicular and parallel to the press direction are 176 and $179\text{ }\mu\text{V K}^{-1}$, respectively. We noticed

that σ and S are highly anisotropic in two directions, so the products of the power factor and temperature are similar as well, peaking around $0.7 \text{ mW m}^{-1} \text{ K}^{-2}$ at $450 \text{ }^\circ\text{C}$, which is about 40% higher compared with the state-of-the-art value in ref 7 at a similar temperature. The peak power factor there was achieved around $240 \text{ }^\circ\text{C}$ instead,⁷ and the value itself is much lower than ours. It is worth noting that almost all of the previously reported semimetal or narrow-band-gap semiconductor dense materials compacted from wet-chemical-synthesized nanostructures show deteriorated power factors, caused by decreases in the electrical conductivity or thermopower.^{3,4,5c,d} For the CCTSe hot-pressed dense material we synthesized, the electrical conductivity is largely enhanced, while the dense material still possesses a high thermopower. The power factors are highly enhanced and can possibly be further improved through further tuning the chemical composition.

Two disk samples were cut from hot-pressed cylinder as well to measure thermal conductivities (κ) parallel and perpendicular to the press direction. Due to the increased phonon scattering at nanocrystalline boundaries and the point defects, the κ values of our hot-pressed sample along both directions are smaller than that of the bulk undoped CCTSe within the measured temperature range. At room temperature, our sample has an isotropic and low thermal conductivity of $1.7 \text{ W m}^{-1} \text{ K}^{-1}$, which is about 40% lower than that of the undoped bulk. The total thermal conductivity decreases rapidly with temperature, which indicates that the lattice thermal conductivity makes the major contribution to κ , since σ increases with temperature. At $450 \text{ }^\circ\text{C}$, the total thermal conductivity along the perpendicular direction is as low as $0.77 \text{ W m}^{-1} \text{ K}^{-1}$, which is about 20% lower than that of the undoped $\text{Cu}_2\text{CdSnSe}_4$ bulk but 50% larger than that of $\text{Cu}_{2.1}\text{Cd}_{0.9}\text{SnSe}_4$ due to the increase in contribution of charge carriers and the lower content of heavy Cd atoms in the total composition. Note that the regrowth of nanoparticles in the dense material is very clear (Figure 2d) during the hot-pressing process; better control of the hot-pressing conditions to reduce the regrowth of nanoparticles might lead to an even lower thermal conductivity. To exclude the contribution of charge carriers in the total thermal conductivity, the Wiedemann–Franz law with a Lorenz number (L_0) of $2.0 \times 10^{-8} \text{ W} \cdot \Omega \text{ K}^{-2}$ is used (electronic contribution $\kappa_{E_r} = L_0 \sigma T$, see Figure S4). After calculation, we found that the lattice thermal conductivity κ_L ($\kappa = \kappa_L + \kappa_{E_r}$) is at least 30% lower than that of the undoped bulk material along both directions, and the reduction in lattice thermal conductivity should be caused by enhanced phonon scatterings at nanocrystalline boundaries and point defect sites. Compared with the κ_L of Cu-doped $\text{Cu}_{2.1}\text{Cd}_{0.9}\text{SnSe}_4$ bulk material at about $450 \text{ }^\circ\text{C}$, the lattice thermal conductivities of the CCTSe nanocomposite we prepared are 50% larger; the increase can possibly be attributed to the lower content of heavy Cd atoms in the total composition, as it has been demonstrated in previous work that the κ_L of CCTSe is very sensitive to variations in composition.⁷

According to the above measured data, we calculated the temperature dependence of ZT values, which is shown in Figure 4b. The ZT values are isotropic below $400 \text{ }^\circ\text{C}$, while the dense sample shows a little bit higher ZT value along the parallel direction at $450 \text{ }^\circ\text{C}$. The ZT value along the perpendicular direction goes from 0.03 to 0.65 with temperature increasing from room temperature to about $450 \text{ }^\circ\text{C}$. The peak ZT value observed at $450 \text{ }^\circ\text{C}$ is much larger than that of undoped bulk polycrystalline CCTSe and equivalent to the state-of-art for $\text{Cu}_{2.1}\text{Cd}_{0.9}\text{SnSe}_4$. The peak ZT value obtained here is larger than

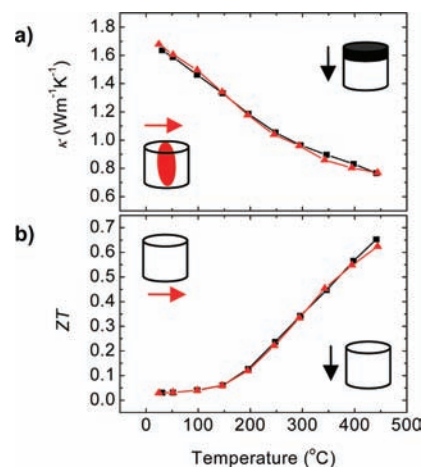


Figure 4. Temperature dependence of (a) thermal conductivity and (b) dimensionless figure-of-merit parallel and perpendicular to the pressing direction. The arrows in figures indicate the directions of the property being measured, the direction of the hot pressing is parallel to black arrows.

for most dense materials compacted from wet-chemistry-synthesized nanocrystals^{4,5c} and the state-of-art values for Cu- or In-doped $\text{Cu}_2\text{ZnSnSe}_4$ and Cu_2SnSe_3 ⁹ at similar temperatures.

To test the repeatability of our results, we prepared another cylinder under the same conditions and studied its transport properties in parallel direction. The results demonstrate that samples from two batches show small discrepancies in individual properties, but an almost consistent peak ZT value of 0.7 was obtained at $450 \text{ }^\circ\text{C}$ (Figure S5). Noting that the powder for hot-pressing into a cylinder was collected from more than 10 reactions, the uncertainties in individual properties are possibly the result of discrepancies in the product among different reactions. Further work toward simplifying the synthetic procedure and scaling-up the output of a single reaction is being carried out. It is possible that the reproducibility can be further improved.

To conclude, we report a solution-based strategy for successful synthesis of monodispersed quaternary CCTSe nanocrystals for the first time and characterize the thermoelectric properties of dense materials compacted from those nanoparticles. We demonstrate a case of wet-chemistry nanostructuring on a wide-band-gap thermoelectric material. Compared to previous reports, a largely enhanced power factor is observed in our wet-chemistry nanostructured dense material, and the peak ZT value reaches 0.65 at $450 \text{ }^\circ\text{C}$, which is equivalent to the state-of-art value for this material at a similar temperature. Further enhancement of the thermoelectric properties can possibly be obtained through fine-tuning the chemical composition and better controlling the grain size during the compacting procedure.

■ ASSOCIATED CONTENT

S Supporting Information. Synthesis and ligand removal procedures, details of thermoelectric properties characterization, ultrathin TEM image and corresponding SAED pattern of the dense material, UV–vis absorption spectrum of nanocrystals, XRD pattern of hot-pressed dense sample, temperature dependence of κ_L , and TE characterization of the repeat samples. This material is available free of charge via the Internet at <http://pubs.acs.org>.

AUTHOR INFORMATION

Corresponding Author

shyu@ustc.edu.cn; zhifeng.ren@bc.edu

Author Contributions

[#]These authors contributed equally to this paper.

ACKNOWLEDGMENT

We acknowledge funding support from the National Basic Research Program of China (2010CB934700), the National Natural Science Foundation of China (Nos. 50732006, 91022032), the International Science & Technology Cooperation Program of China (2010DFA41170), and a Principle Investigator Award from the National Synchrotron Radiation Laboratory at the University of Science and Technology of China. We thank Prof. Yang Jiang and Ling Han at Hefei University of Technology for their help in hot-pressing. The work performed at Boston College is funded by the U.S. Department of Energy under contract no. DOE DE-FG02-00ER45805 (Z.F.R.).

REFERENCES

- (1) (a) Boukai, A. I.; Bunimovich, Y.; Tahir-Kheli, J.; Yu, J. K.; Goddard, W. A.; Heath, J. R. *Nature* **2008**, *451*, 168. (b) Chung, D. Y.; Hogan, T.; Brazis, P.; Rocci-Lane, M.; Kannewurf, C.; Bastea, M.; Uher, C.; Kanatzidis, M. G. *Science* **2000**, *287*, 1024. (c) Poudel, B.; Hao, Q.; Ma, Y.; Lan, Y. C.; Minnich, A.; Yu, B.; Yan, X.; Wang, D. Z.; Muto, A.; Vashaee, D.; Chen, X. Y.; Liu, J. M.; Dresselhaus, M. S.; Chen, G.; Ren, Z. *Science* **2008**, *320*, 634. (d) Hsu, K. F.; Loo, S.; Guo, F.; Chen, W.; Dyck, J. S.; Uher, C.; Hogan, T.; Polychroniadis, E. K.; Kanatzidis, M. G. *Science* **2004**, *303*, 818. (e) Heremans, J. P.; Jovovic, V.; Toberer, E. S.; Saramat, A.; Kurosaki, K.; Charoenphakdee, A.; Yamanaka, S.; Snyder, G. J. *Science* **2008**, *321*, 554. (f) Rhyee, J. S.; Lee, K. H.; Lee, S. M.; Cho, E.; Il Kim, S.; Lee, E.; Kwon, Y. S.; Shim, J. H.; Kotliar, G. *Nature* **2009**, *459*, 965. (g) Pei, Y. Z.; Shi, X. Y.; LaLonde, A.; Wang, H.; Chen, L. D.; Snyder, G. J. *Nature* **2011**, *473*, 66.
- (2) (a) Vineis, C. J.; Shakouri, A.; Majumdar, A.; Kanatzidis, M. G. *Adv. Mater.* **2010**, *22*, 3970. (b) Kanatzidis, M. G. *Chem. Mater.* **2010**, *22*, 648.
- (3) Son, J. S.; Park, K.; Han, M. K.; Kang, C.; Park, S. G.; Kim, J. H.; Kim, W.; Kim, S. J.; Hyeon, T. *Angew. Chem., Int. Ed.* **2011**, *50*, 1363.
- (4) (a) Scheele, M.; Oeschler, N.; Meier, K.; Kornowski, A.; Klinke, C.; Weller, H. *Adv. Funct. Mater.* **2009**, *19*, 3476. (b) Dirmeyer, M. R.; Martin, J.; Nolas, G. S.; Sen, A.; Badding, J. V. *Small* **2009**, *5*, 933.
- (5) (a) Datta, A.; Paul, J.; Kar, A.; Patra, A.; Sun, Z. L.; Chen, L. D.; Martin, J.; Nolas, G. S. *Cryst. Growth Des.* **2010**, *10*, 3983. (b) Kovalenko, M. V.; Spokoyny, B.; Lee, J. S.; Scheele, M.; Weber, A.; Perera, S.; Landry, D.; Talapin, D. V. *J. Am. Chem. Soc.* **2010**, *132*, 6686. (c) Zhao, Y. X.; Dyck, J. S.; Hernandez, B. M.; Burda, C. *J. Am. Chem. Soc.* **2010**, *132*, 4982. (d) Scheele, M.; Oeschler, N.; Veremchuk, I.; Reinsberg, K. G.; Kreuziger, A. M.; Kornowski, A.; Broekaert, J.; Klinke, C.; Weller, H. *ACS Nano* **2010**, *4*, 4283.
- (6) Zhang, Y. C.; Wang, H.; Kraemer, S.; Shi, Y. F.; Zhang, F.; Snedaker, M.; Ding, K. L.; Moskovits, M.; Snyder, G. J.; Stuck, G. D. *ACS Nano* **2011**, *5*, 3158.
- (7) Liu, M. L.; Chen, I. W.; Huang, F. Q.; Chen, L. D. *Adv. Mater.* **2009**, *21*, 3808.
- (8) (a) Shi, X. Y.; Huang, F. Q.; Liu, M. L.; Chen, L. D. *Appl. Phys. Lett.* **2009**, *94*, 122103. (b) Liu, M. L.; Huang, F. Q.; Chen, L. D.; Chen, I. W. *Appl. Phys. Lett.* **2009**, *94*, 202103.
- (9) Shi, X. Y.; Xi, L. L.; Fan, J.; Zhang, W. Q.; Chen, L. D. *Chem. Mater.* **2010**, *22*, 6029.
- (10) Guo, Q.; Ford, G. M.; Hillhouse, H. W.; Agrawal, R. *Nano Lett.* **2009**, *9*, 3060.
- (11) Panthani, M. G.; Akhavan, V.; Goodfellow, B.; Schmidtke, J. P.; Dunn, L.; Dodabalapur, A.; Barbara, P. F.; Korgel, B. A. *J. Am. Chem. Soc.* **2008**, *130*, 16770.
- (12) (a) Guo, Q. J.; Hillhouse, H. W.; Agrawal, R. *J. Am. Chem. Soc.* **2009**, *131*, 11672. (b) Steinhagen, C.; Panthani, M. G.; Akhavan, V.; Goodfellow, B.; Koo, B.; Korgel, B. A. *J. Am. Chem. Soc.* **2009**, *131*, 12554.
- (13) (a) Volobujeva, O.; Raudoja, J.; Mellikov, E.; Grossberg, M.; Bereznev, S.; Traksmaa, R. *J. Phys. Chem. Solids* **2009**, *70*, 567. (b) Altosaar, M.; Raudoja, J.; Timmo, K.; Danilson, M.; Grossberg, M.; Krustok, J.; Mellikov, E. *Phys. Status Solidi A: Appl. Mater.* **2008**, *205*, 167.
- (14) (a) Yang, C. C.; Li, S. *J. Phys. Chem. B* **2008**, *112*, 14193. (b) Zeiri, L.; Patla, I.; Acharya, S.; Golan, Y.; Efrima, S. *J. Phys. Chem. C* **2007**, *111*, 11843.